INTERNATIONAL JOURNAL FOR NUMERICAL METHODS IN FLUIDS, VOL. 24, 787–807 (1997)

NUMERICAL MODELLING OF THREE-DIMENSIONAL FLY-ASH FLOW IN POWER UTILITY BOILERS

J. Y. TU* AND C. A. J. FLETCHER

Centre for Advanced Numerical Computation in Engineering and Science (CANCES), University of New South Wales, Sydney, 2052, Australia

AND

M. BEHNIA

School of Mechanical and Manufacturing Engineering, University of New South Wales, Sydney, N.S.W. 2052, Australia

SUMMARY

A two-fluid Eulerian model in combination with a particle–wall collision model and generalized Eulerian boundary conditions for the particulate phase is employed to predict complex three-dimensional fly-ash flows which often cause severe erosion to boiler tubes located in power utility boilers. Mean momentum and mass conservation equations are solved for each phase using a finite volume scheme with two-way coupling and a modified renormalization group (RNG)-based k–ε turbulence model. Comparison of predicted particle concentration with measured data is made and excellent agreement is obtained. The detailed character of the particulate velocity field and concentration just downstream of the 180° bend shows a marked dependence on the Stokes number not previously reported. © 1997 by John Wiley & Sons, Ltd.

KEY WORDS: three-dimensional; two-phase flow; Eulerian modelling; RNG k–ε turbulence model; particle–wall collision; power utility boilers

1. INTRODUCTION

Burning coal for electricity generation creates products of combustion which contain solid particles (fly-ash). These small solid particles are carried by the hot (flue) gas flow through the heat exchanger in a power utility boiler. The transported fly-ash can cause severe erosion to the heat exchanger boiler tubes, especially in the economizer. Such solid particles in suspension may also significantly influence the heat transfer characteristics of boiler heat exchangers. Current interest in design, operation and maintenance of energy conversion systems has led to a considerable research activity in modelling turbulent particle-laden gas flows. Reducing erosion and enhancing heat transfer in the design of tube banks and heat exchangers located in power utility boilers are crucial for their efficient operation. The annual cost of erosion to a plant operator can be as high as several million dollars. Therefore it is important to investigate the hydrodynamics of fluid and particle motion for a better understanding of tube bundle erosion and the influence of the presence of solid particles on the fluid flow, which may affect the heat transfer performance.

Despite recognition of the operational importance, the complexity of the flow generated within a power utility boiler (three-dimensional, two-phase and turbulent) has compelled designers to make

* Present address: Australian Nuclear Science and Technology Organisation, P.M. Bag 1, NSW 2234, Australia.

CCC 0271–2091/97/080787–20 $17.50

Received January 1995
Revised January 1996

use of empirical information and often complement that with pilot plant experiments in order to tackle the problems associated with erosion reduction,[1] heat transfer enhancement[2] and the design of new boiler heat exchangers.[3] This is a rather expensive and inefficient procedure, sometimes valid for a very restricted parameter range. Thus it is desirable to develop computer codes that predict in considerable detail and accuracy the flow field within power utility boilers under different operating conditions.

Numerical investigations of two-phase flows in various geometries, rather than specifically in power utility boilers, are many and varied. A comprehensive review of the alternative approaches currently employed in predicting particle-laden turbulent flows has been recently provided by Elghobashi[4]. Historically, two main approaches can be distinguished in the computational analysis of the dispersed phase. In the Lagrangian approach (or trajectory model) the trajectories of individual particles are calculated based on varying initial conditions, whereas in the Eulerian approach (or two-fluid model) the particulate phase is treated as a continuum subject to appropriate boundary conditions. The Lagrangian approach is a more fundamental procedure to describe the particle–wall collision process. It can yield a detailed physical description of the individual particles, such as particle speeds and trajectories, and can be easily used for polydispersed flows.

The major shortcoming of using a Lagrangian approach is that some of these features rely on a deterministic approach which requires unreasonably detailed and unaffordably expensive computations. Also, the particle paths which result from a Lagrangian prediction often do not contain enough information for design engineers. From an engineering design perspective the mean particulate flow fields need to be known in terms of mean particulate velocities and the distribution of particle concentration to facilitate quantifiable decisions. Therefore the continuum model (Eulerian approach) becomes attractive as an alternative way of representing the particulate phase to obtain the mean particulate flow fields. In addition, the effects of interactions between the two phases (two-way coupling) are more easily considered by using the Eulerian approach.[5–7]

Most applications of two-fluid models are limited to geometrically simple cases and two-dimensions, such as vertical pipe flows[6,8] and free jets,[5,9] and some are only for laminar conditions and lower-inertial particulate flows.[10–12] Recently, Reeks[13] has derived the conservation equations of the dispersed phase from a kinetic equation analogous to the Maxwell–Boltzmann equation and Simonin *et al.*[14] carried out a large-eddy simulation similar to the Reeks analysis. However, both investigations are restricted to the analysis of simple model problem, i.e. Couette flow. One of the difficulties for complex gas–particle flows using a two-fluid model is of setting appropriate boundary conditions at solid wall surfaces and modelling the particle–wall interactions under the Eulerian formulation for low-loading particulate phase.

This problem has been resolved[15,16] by establishing a set of Eulerian formulation, generalized wall boundary conditions and by developing a particle–wall collision model to represent particle–wall momentum transfers. Then complex two-phase flow, where the mean particulate flow behaviour near the surface of a wall depends significantly on the interaction of particles with the solid wall, can be simulated appropriately. The numerical predictions using the developed model for complex flow domains have been verified extensively with the available laboratory experiments, such as Schweitzer and Humphrey's data[17] for gas–particle flow past one tube,[15] Kliafas and Holt's data[18] for turbulent gas–solid flow in a 90° squares section bend,[16] Morsi *et al.*'s measurements[19] of turbulent particle-laden gas flows in an in-line tube bank[20] as well as the data of Tsuji *et al.*[21] for vertical pipe two-phase flows including particulate turbulence modulation.[7]

The present paper describes a general three-dimensional calculation procedure based on the two-fluid model[5,6] in combination with the developed particle–wall collision model and the generalized Eulerian boundary conditions for the particulate phase and present its application to predicting complex three-dimensional fly-ash flow in power utility boilers. The typical flow characteristics of a

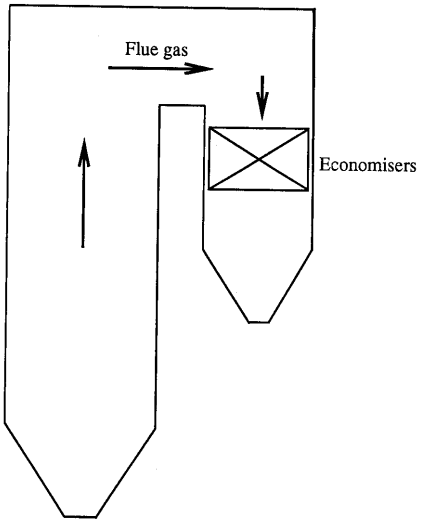

Figure 1. Simplified arrangement of a typical power utility

power utility boiler are that the fly-ash entrained in the gas stream is 'centrifuged' and flung to a side wall because of the 180° bend in the flow path at the top of the boiler (see Figure 1, which illustrates a simplified arrangement of a typical power utility boiler). The velocities of both gas and particulate phases are highest in this region. Owing to the different inertia, the larger the particles are, the more particles are flung to the right side of the economizer inlet. This creates a region of high fly-ash loading and high velocity towards the right side wall above the economizer tube bank. Comparison of predicted particle concentration with measured data[22] shows excellent agreement. However, this essentially two-dimensional character is further modified by the constraining effect of the end walls, generating very complex particulate concentration distributions (Section 3).

The next section provides a description of the mathematical model, including (i) assumptions made, (ii) governing equations for both gas and particulate phases where gas–particle and particle–wall interactions are allowed, (iii) RNG-based k–ε turbulence models considering the extra dissipation (two-way coupling) due to the presence of particulate phase, (iv) boundary conditions of both phases and (v) the numerical solution procedure. We shall then present detailed three-dimensional predictions in terms of mean fly-ash velocity and concentration for different particle sizes in two configurations of power utility boilers. Conclusions and final remarks are provided in the last section.

2. MATHEMATICAL MODEL

2.1. Governing equations

In this subsection we present the assumptions made and the forms of the governing equations adopted for predicting turbulence fly-ash flows in power utility boilers. The main assumptions implied in the present study are as follows.

1. The particulate phase is dilute but continuous and comprised of monodisperse spherical particles, the fluid phase is Newtonian and the physical properties of each phase are constant.

2. Particle–particle interactions are neglected, but the effect of the particle–wall collision on the particulate phase is considered and fluid–particle two-way interaction is allowed. Forces due to the gas pressure gradient, Magnus forces due to particle rotation and Saffman forces due to the viscous shear rate on the particulate phase are negligible.
3. The mean flow is steady, three-dimensional, incompressible and isothermal. The turbulent flow is locally isotropic.
4. The third-order correlations involving fluctuations in the particulate phase concentration are negligible.

The criteria for which these assumptions as well as the continuum approach conditions are valid have been discussed in the literature.[23,24] The derivation of the governing equations in the Eulerian formulation is given by Drew;[25] only a summary of these equations is presented here.

2.1.1. Gas phase. The governing equations in Cartesian form for the mean turbulent gas flow are obtained by applying the Reynolds decomposition and time averaging the instantaneous continuity and momentum equations:

$$\frac{\partial}{\partial x_i}(\rho_g u_g^i) = 0, \tag{1}$$

$$\frac{\partial}{\partial x_j}(\rho_g u_g^i u_g^i) = -\frac{\partial P}{\partial x_i} + \frac{\partial}{\partial x_j}\left(\rho_g \nu_{gl} \frac{\partial}{\partial x_j} u_g^i\right) - \frac{\partial}{\partial x_j}(\rho_g \overline{u_g' u_g'^j}) - F_D^i, \tag{2}$$

where ρ_g, u_g, u_g' and P are the bulk density, mean velocity, fluctuating velocity and mean pressure of the gas phase respectively, ν_{gl} is the gas laminar viscosity and F_D is the aerodynamic drag force due to the slip velocity between the two phases, which will be described later.

2.1.2. Particulate phase. As with the gas phase, it is the mean behaviour that is of primary practical importance. After Reynolds averaging, the steady form of the governing equations for the particulate phase is

$$\frac{\partial}{\partial x_i}(\rho_p u_p^i) = -\frac{\partial}{\partial x_i}(\overline{\rho_p' u_p'^i}), \tag{3}$$

$$\frac{\partial}{\partial x_j}(\rho_p u_p^i u_p^j) = -\frac{\partial}{\partial x_j}(\rho_p \overline{u_p'^i u_p'^j} + u_p^j \overline{\rho_p' u_p'^i} + u_p^i \overline{\rho_p' u_p'^j}) + F_G^i + F_D^i + F_{WM}^i, \tag{4}$$

where ρ_p is the mass of particles per unit volume of mixture (or 'bulk density' of the particulate phase, where $\rho_p = \alpha_p \rho_s$, α_p is the volume fraction of the particulate phase and ρ_s is the particle material density). It may be noted that owing to the dilute particulate phase assumptions, the multiplication of each term in the equations for the gas phase by $1 - \alpha_p$ is replaced by unity. u_p and u_p' are the mean velocity and fluctuating velocity of the particulate phase respectively.

In equation (4) there are three additional terms representing the gravity force, the aerodynamic drag force and the wall momentum transfer force due to particle–wall collision respectively. The gravity force is $F_G = \rho_p g$, where g is the gravitational acceleration. The drag force F_D due to the slip velocity of the two phases is defined by

$$F_D^i = \rho_p \frac{f(u_g^i - u_p^i)}{t_p}, \tag{5}$$

where the correction factor f selected according to Schuh *et al.*[26] is

$$f = \begin{cases} 1 + 0{\cdot}15Re_{\mathrm{p}}^{0{\cdot}687}, & 0 < Re_{\mathrm{p}} \leqslant 200, \\ 0{\cdot}914Re_{\mathrm{p}}^{0{\cdot}282} + 0{\cdot}0135Re_{\mathrm{p}}, & 200 < Re_{\mathrm{p}} \leqslant 2500, \\ 0{\cdot}0167Re_{\mathrm{p}}, & 2500 < Re_{\mathrm{p}}, \end{cases} \tag{6}$$

with the particulate Reynolds number defined by

$$Re_{\mathrm{p}} = \frac{|u_{\mathrm{g}}^i - u_{\mathrm{p}}^i| d_{\mathrm{p}}}{v_{\mathrm{gl}}}, \tag{7}$$

and the particle response or relaxation time is

$$t_{\mathrm{p}} = \frac{\rho_{\mathrm{s}} d_{\mathrm{p}}^2}{18 \rho_{\mathrm{g}} v_{\mathrm{gl}}}, \tag{8}$$

with d_{p} the diameter of the particle.

For a dilute suspension the viscous and pressure terms in the particulate phase momentum equations are neglected. It may be noted that for the large particles or high Stokes number the particulate flow will be little influenced by the turbulence and the aerodynamic drag of the carrier phase. The main controlling factor for this type of particulate flow will be the particle–wall interaction process. The wall momentum transfer force due to particle–wall interaction is given by[15,16]

$$F_{\mathrm{WM}}^{\mathrm{N}} = -C_{\mathrm{N}}[1 + (\bar{e}_{\mathrm{p}}^{\mathrm{N}})^2] \rho_{\mathrm{p}} |W_{\mathrm{p},h}^{\mathrm{N}}| W_{\mathrm{p},h}^{\mathrm{N}} (B^{\mathrm{N}})^2 A_{\mathrm{n}} \tag{9}$$

in the normal direction and

$$F_{\mathrm{WM}}^{\mathrm{T}} = -C_{\mathrm{T}}[1 - (\bar{e}_{\mathrm{p}}^{\mathrm{T}})^2] \rho_{\mathrm{p}} |W_{\mathrm{p},h}^{\mathrm{T}}| W_{\mathrm{p},h}^{\mathrm{T}} (B^{\mathrm{T}})^2 A_{\mathrm{n}} \tag{10}$$

in the tangential direction. Here A_{n} denotes a face area of the control volume coincident with the wall, $\bar{e}_{\mathrm{p}}^N$ and $\bar{e}_{\mathrm{p}}^T$ are the normal and tangential mean restitution coefficients respectively, $W_{\mathrm{p},h}^{\mathrm{N}}$ and $W_{\mathrm{p},h}^{\mathrm{T}}$ are the normal and tangential mean velocities of the particulate phase at a distance h away from the wall respectively and B^{N} and B^{T} are constants related to the restitution coefficients as given by equation (34). C_{N} and C_{T} are coefficients which are modelled by

$$C_{\mathrm{N}} = C_{\mathrm{m}} \frac{W_{\mathrm{p},h}^{\mathrm{N}}}{\left(\sum_{i=1}^{3} (u_{\mathrm{p},h}^i)^2 \right)^{1/2}}, \tag{11}$$

where C_{m} is referred to as the particle inertial impacting efficiency and is similar to that obtained by Ilias and Douglas[27] based in the particle inertia (Stokes number St) and the Reynolds number of the gas phase.

The coefficient C_{T} is related to the tangential wall momentum exchange and is modelled as

$$C_{\mathrm{T}} = \begin{cases} C_{\mathrm{N}}/y^+ & \text{for } y^+ \leqslant 11{\cdot}63, \\ C_{\mathrm{N}} \kappa / \ln(Ey^+) & \text{for } y^+ > 11{\cdot}63, \end{cases} \tag{12}$$

where κ and E are the same as in the turbulence model of the gas phase,[28] 0·41 and 9·0 respectively, and y^+ is a similar definition but for the particulate flow.[29] Alternatively, the tangential coefficient C_{T} can be modelled by relating it to the wall friction.[30] The effect of both normal and tangential wall

momentum exchanges on the particulate flow is only considered for control volumes immediately adjacent to the wall.

2.2. Turbulence models

In the governing equations of both gas and particulate phases there are more unknowns than equations owing to the loss of information inherent in the averaging process. The second-order correlation terms $\overline{u'^i_{\rm g} u'^j_{\rm g}}$, $\overline{u'^i_{\rm g} u'^i_{\rm p}}$, $\overline{u'^i_{\rm p} u'^j_{\rm p}}$ and $\overline{\rho'_{\rm p} u'_{\rm p}}$, which are turbulence fluxes of momentum and mass, require modelling.

For the carrier gas phase, when the eddy viscosity model is used, the Reynolds stresses are

$$\overline{u'^i_{\rm g} u'^j_{\rm g}} = -\nu_{\rm gt}\left(\frac{\partial u^i_{\rm g}}{\partial x_j} + \frac{\partial u^j_{\rm g}}{\partial x_i}\right) + \tfrac{2}{3} k \delta_{ij}, \tag{13}$$

where $\nu_{\rm gt}$ is the turbulent of 'eddy' viscosity of the gas phase and is evaluated as $\nu_{\rm g,eff} - \nu_{\rm gl}$, with the effective viscosity $\nu_{\rm g,eff}$ computed by

$$\nu_{\rm g,eff} = \nu_{\rm gl}\left[1 + \sqrt{\left(\frac{C_\mu}{\nu_{\rm gl}}\right)}\frac{k}{\sqrt{\varepsilon}}\right]^2. \tag{14}$$

The turbulence kinetic energy k and its dissipation rate ε are governed by separate transport equations. A recently developed turbulence model, the dynamic renormalization group theory (RNG)-based k–ε turbulence model,[31] is employed. The RNG-based k–ε turbulence model contains very few empirically adjustable parameters and is therefore applicable to a wide range of flow situations. RNG theory models the k- and ε-transport equations modified by the consideration of particulate turbulence modulation as

$$\frac{\partial}{\partial x_i}(\rho_{\rm g} u^i_{\rm g} k) = \frac{\partial}{\partial x_i}\left(\alpha \rho_{\rm g} \nu_{\rm gt}\frac{\partial k}{\partial x_i}\right) + P_k - \rho_{\rm g}\varepsilon + S_k, \tag{15}$$

$$\frac{\partial}{\partial x_i}(\rho_{\rm g} u^i_{\rm g} \varepsilon) = \frac{\partial}{\partial x_i}\left(\alpha \rho_{\rm g} \nu_{\rm gt}\frac{\partial \varepsilon}{\partial x_i}\right) + \frac{\varepsilon}{k}(C_{\varepsilon 1} P_k - C_{\varepsilon 2}\rho_g \varepsilon) - \rho_{\rm g} R + S_\varepsilon, \tag{16}$$

where α is an inverse Prandtl number which may be obtained from the equation[32]

$$\left|\frac{\alpha - 1{\cdot}3929}{\alpha_0 - 1{\cdot}3929}\right|^{0{\cdot}6321}\left|\frac{\alpha + 2{\cdot}3920}{\alpha_0 + 2{\cdot}3929}\right|^{0{\cdot}3679} = \frac{\nu_{\rm gl}}{\nu_{\rm g,eff}}, \tag{17}$$

with $\alpha_0 = 1$. The turbulence production P_k is evaluated by

$$P_k = \rho_{\rm g}\nu_{\rm gt}\left(\frac{\partial u^i_{\rm g}}{\partial x_j} + \frac{\partial u^j_{\rm g}}{\partial x_i}\right)\frac{\partial u^i_{\rm g}}{\partial x_j}. \tag{18}$$

The rate-of-strain term R in the ε-equation is expressed as

$$R = \frac{C_\mu \eta^3 (1 - \eta/\eta_0)}{1 + \beta\eta^3}\frac{\varepsilon^2}{k}, \qquad \eta = \frac{k}{\varepsilon}(2S^2_{ij})^{1/2}, \qquad S_{ij} = \frac{1}{2}\left(\frac{\partial u^i_{\rm g}}{\partial x_j} + \frac{\partial u^j_{\rm g}}{\partial x_i}\right), \tag{19}$$

where $\beta = 0{\cdot}015$ and $\eta_0 = 4{\cdot}38$. According to RNG theory,[31] the constants in the turbulent transport equations are $C_\mu = 0{\cdot}0845$, $C_{\varepsilon 1} = 1{\cdot}42$ and $C_{\varepsilon 2} = 1{\cdot}68$ respectively.

For gas–particle two-phase flow it is generally accepted that the presence of particles (particle diameter less than 200 μm)[33] absorbs some of the turbulent energy present in the carrier gas flow. The effect is typically modelled with extra dissipation terms S_k and S_ε in the k- and ε-transport equations respectively. For confined two-phase flow the effects of the particulate phase on the turbulence structure of the gas phase ($-\overline{u_g'^i F_D'^i}$) are modelled by[7]

$$S_k = -2k(\rho_p/t_p)[1 - \exp(-B_k t_p/t_L)] \tag{20}$$

in the k-equation and

$$S_\varepsilon = -2\varepsilon(\rho_p/t_p)[1 - \exp(-B_\varepsilon t_p/t_L)] \tag{21}$$

in the ε-equation, where $B_k = 0{\cdot}09$, $B_\varepsilon = 0{\cdot}4$ and $t_L = k/\varepsilon$.

The second-order correlation terms in the governing equations of the particulate phase using a gradient hypothesis[5,6] are

$$-\overline{\rho_p' u_p'^i} = D_p \frac{\partial \rho_p}{\partial x_i}, \qquad -\overline{u_p'^i u_p'^j} = \nu_p \left(\frac{\partial u_p^i}{\partial x_j} + \frac{\partial u_p^j}{\partial x_i} \right), \tag{22}$$

where the particulate turbulent diffusivities D_p and ν_p are related to the turbulent viscosity of the gas phase, ν_{gt}, by

$$D_p = \frac{\nu_p}{Sc}, \qquad \nu_p = K_p \nu_{gt}, \tag{23}$$

where Sc is the turbulent Schmidt number, taken to be $0{\cdot}7$. K_p is a weight factor accounting for the particle inertia and is given by

$$K_p = \max[K_d, 1/(1 + St^t)], \tag{24}$$

where K_d is a numerical dissipation and St^t is the turbulent Stokes number, equal to t_p/t_e. Here the turbulent eddy characteristic time follows the work of Adeniji-Fashola and Chen[6] for confined two-phase flow, i.e. $t_e = 0{\cdot}125k/\varepsilon$. Thus K_p reflects the transfer of turbulent energy to the particulate phase due to the particle inertia. In some regions, particularly near the wall, this value becomes very small (less than $0{\cdot}001$), so that K_d is taken to be $0{\cdot}01$ to avoid numerical instability, because the particulate flow with less than 1% turbulent diffusivity of the gas turbulent viscosity is already convection-dominated. The isotropic nature of the turbulent diffusivities in (22) and (23) is open to criticism.[13] However, the influence of this assumption is rather small for the geometrically complex, three-dimensional flows considered in Section 3.

2.3. Generic transport form for two-phase flow

The governing equations of both gas and particulate phases can be finally written in a generic transport form as[34]

$$\frac{\partial}{\partial x_j}(A_j \phi) - \frac{\partial}{\partial x_j}\left(B \frac{\partial \phi}{\partial x_j} \right) = S, \tag{25}$$

which can be solved efficiently using a high-order finite volume discretization.[35]

2.3.1. Gas phase. Continuity equation ($\phi = 1$):

$$A_j = \rho_g u_g^j, \qquad B = 0, \qquad S = 0. \tag{26}$$

Momentum equation ($\phi = u_g^i$):

$$A_j = \rho_g u_g^j, \qquad B = \rho_g v_{g,\text{eff}}, \qquad S = -\frac{\partial P}{\partial x_i} - F_D^i. \tag{27}$$

Turbulent kinetic energy equation ($\phi = k$):

$$A_j = \rho_g u_g^j, \qquad B = \alpha \rho_g v_{gt}, \qquad S = P_k - \rho_g \varepsilon + S_k. \tag{28}$$

ε-Equation ($\phi = \varepsilon$):

$$A_j = \rho_g u_g^j, \qquad B = \alpha \rho_g v_{gt}, \qquad S = \frac{\varepsilon}{k}(C_{\varepsilon 1} P_k - C_{\varepsilon 2} \rho_g \varepsilon) - R + S_\varepsilon. \tag{29}$$

2.3.2. Particulate phase. Continuity equation ($\phi = \rho_p$):

$$A_j = \rho_p u_p^j, \qquad B = \rho_p D_p, \qquad S = \left(\rho_p u_p^i - D_p \frac{\partial \rho_p}{\partial x_i}\right) \frac{\partial \rho_p}{\partial x_i}. \tag{30}$$

Momentum equation ($\phi = u_p^i$):

$$A_j = \rho_p u_p^j, \quad B = \rho_p v_p, \quad S = \frac{\partial}{\partial x_j}\left(\rho_p v_p \frac{\partial u_p^j}{\partial x_i}\right) + \frac{\partial}{\partial x_j}\left[D_p\left(u_p^j \frac{\partial \rho_p}{\partial x_i} + u_p^i \frac{\partial \rho_p}{\partial x_j}\right)\right] + F_D^i + F_G^i + F_{WM}^i. \tag{31}$$

2.4. Boundary conditions

The boundary conditions at the inlet are specified for all dependent variables in both gas and particulate phases. At the outflow the normal gradient of these quantities is set to zero. A 'no-slip' boundary condition is employed for the gas velocity at the wall surface. The boundary conditions at the solid wall for the particular phase are based on the generalized wall boundary equations, which can be written in a generic form as[15,16]

$$a\varphi_w + b\left(\frac{\partial \varphi}{\partial n}\right)_w = c, \qquad \varphi = [W_p^N, W_p^T, \rho_p], \tag{32}$$

where n indicates the direction normal to the surface of the wall. The coefficients in the equation can be determined as

$$\begin{aligned} a_N &= A^N - B^N, & b_N &= A^N K n_h, & c_N &= 0, \\ a_T &= A^T - B^T, & b_T &= A^T K n_h, & c_T &= 0, \\ a_\rho &= B^N - A^N, & b_\rho &= A^N K n_h, & c_\rho &= 0, \end{aligned} \tag{33}$$

with

$$\begin{aligned} A^N &= \left(\frac{1{\cdot}0 + \bar{e}_p^N(-\bar{e}_p^N)^q}{2}\right)^{1/(q+1)}, & A^T &= \left(\frac{1{\cdot}0 + (\bar{e}_p^T)^{q+1}}{2}\right)^{1/(q+1)}, \\ B^N &= \left(\frac{\bar{e}_p^N[1{\cdot}0 + (-\bar{e}_p^N)^q]}{1{\cdot}0 + \bar{e}_p^N}\right)^{1/(q+1)}, & B^T &= \left(\frac{\bar{e}_p^N + (\bar{e}_p^T)^{q+1}}{1{\cdot}0 + \bar{e}_p^N}\right)^{1/(q+1)}, \end{aligned} \tag{34}$$

where q is a factor required for the averaging process, $1 \leqslant q \leqslant 2$; $q = 1$ refers to a momentum average and $q = 2$ corresponds to an energy average. Kn_h is a Knudsen number defined by the gas–particle interaction length l_{gp} divided by the system characteristic length L_s, i.e. $Kn_h = h(l_{gp}/L_s)$. For turbulent flow,[29] $l_{gp} = t_p|W'_R|$, where $|W'_R|$ is the modulus of the relative turbulence intensity between the gas and the particulate phase.

2.5. Numerical procedure

Equation (25) is discretized using a finite volume formulation in generalized co-ordinate space with the metric information expressed in terms of area vectors. The equations are solved on a non-staggered grid. The velocity components in fixed Cartesian directions are treated as scalars after the transformation from physical co-ordinates to computational space co-ordinates. To approximate the convective terms at faces of the control volumes, a generalized QUICK convective differencing method[36] is used. Second derivatives are evaluated using three-point symmetric formulae. Each governing equation is sequentially relaxed to update one of the primitive variables. A velocity potential correction[37] is introduced to satisfy continuity of the gas phase and upgrade the gas pressure using a modified SIMPLE algorithm.[38] The stored values at the centroids are interpolated and modified to calculate the flow flux at faces of the control volumes using the moment interpolation method.[39] The governing equations for both gas and particulate phases are solved sequentially at each iteration to obtain all the dependent variables. At each global iteration each equation is iterated using a strongly implicit procedure.[40]

3. RESULTS AND DISCUSSION

In this section the detailed three-dimensional fly-ash flow patterns in two boiler models, a generic and a more realistic model, are presented and discussed. The flow conditions for computations of both cases are chosen to be as close as possible to the operational conditions in a power station where some measurements were carried out.[22] The following operating conditions are assumed: gas density $\rho_g = 1{\cdot}17$ kg m^{-3}; kinematic viscosity of gas, $\nu_{gl} = 1{\cdot}68 \times 10^{-5}$ m^2 s^{-1}; uniform vertical inlet velocity of both phases, $U_{in} = 10$ m s^{-1}; inlet turbulence intensity $Tu_{in} = 5\%$; particle material density (fly-ash) $\rho_s = 1500$ kg m^{-3}; mean restitution coefficients $\bar{e}_p^N = \bar{e}_p^T = 0{\cdot}9$; particle mass loading ratio $\beta = 0{\cdot}1$ kg kg^{-1}; particle sizers $d_p = 5$, 10, 30, 50, 80, 100 μm.

3.1. Boiler configuration I

A three-dimensional schematic diagram of a generic model of a power utility boiler (boiler configuration I) is shown in Figure 2. The computational control volumes used for this case consist of $62 \times 52 \times 32$ points in directions I, J and K respectively. Figure 3 shows the numerical prediction of fly-ash flow through the boiler in terms of mean particulate velocity streamlines (i.e. mean particle trajectories) at various plane sections in the K-direction (depth of boiler). As we can see, for very small particles the particulate flow will follow the velocity streamlines of the gas phase even in the presence of complex domains such as a 180° bend boiler configuration. This is because the small particles promptly follow the carrier fluid after a collision with the bounded wall and the centrifugal effects on the lower-inertia particles are less important than the aerodynamic drag from the carrier phase. Thus, for the particle size $d_p = 5$ μm corresponding to a Stokes number $St = 0{\cdot}004$, this implies that the prediction of the particulate flow also gives the carrier flow behaviour. In the case of large particles (e.g. $d_p = 100$ μm corresponding to $St = 0{\cdot}8$), their motion is dominated by inertia and not strongly influenced by flow turbulence. Such large particles also respond slowly to changes in the

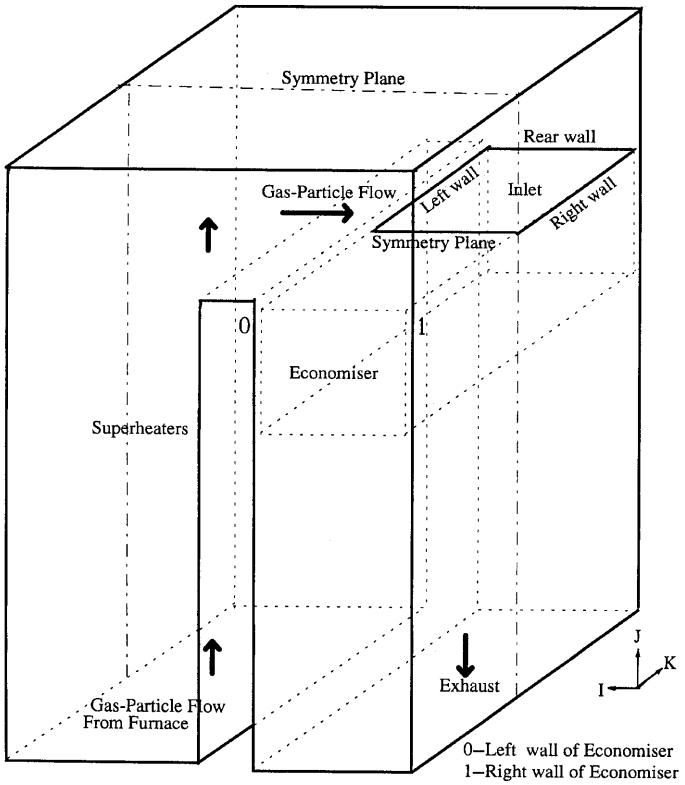

Figure 2. 3D schematic diagram of boiler model I

mean flow, so that their motion is considerably influenced by the centrifugal effect and the wall collision process. Owing to their inertia, the particles maintain their direction of motion after turning, which results in their deviation from the mean flow of the carrier fluid.

Note that the result for the gas phase presented in Figure 3 is a two-phase result (two-way coupling) with a particle size $d_p = 5\ \mu$m. For such a low Stokes number the particles have entirely followed the gas flow. The results for the gas phase when the particles correspond to larger Stokes numbers are not shown in the figure. Actually, for the current particle loading (at the loading ratio $0{\cdot}1$ kg kg^{-1} the real operating condition in power boiler varies between $0{\cdot}02$ and $0{\cdot}06$), the influence of the particulate phase on the mean streamlines of the gas phase is not significant.

It is also found that the mean streamlines of both gas and particulate phases are very different between the sections away from and near the rear wall. The gas and particulate flows are significantly influenced by the presence of the rear wall and become very complex. However, it can be seen from the symmetry plane that the smaller fly-ash particles are more influenced by the gas flow and, with increasing particle size, the larger fly-ash particles are accelerated by the centrifugal force and flung to the right-hand side of the economizer inlet. If one counts the number of particles entering the economizer, it is expected that more particles with a larger size will be found at the right-hand side of the economizer inlet. This has been observed from experimental measurements[22] and also from the present computations.

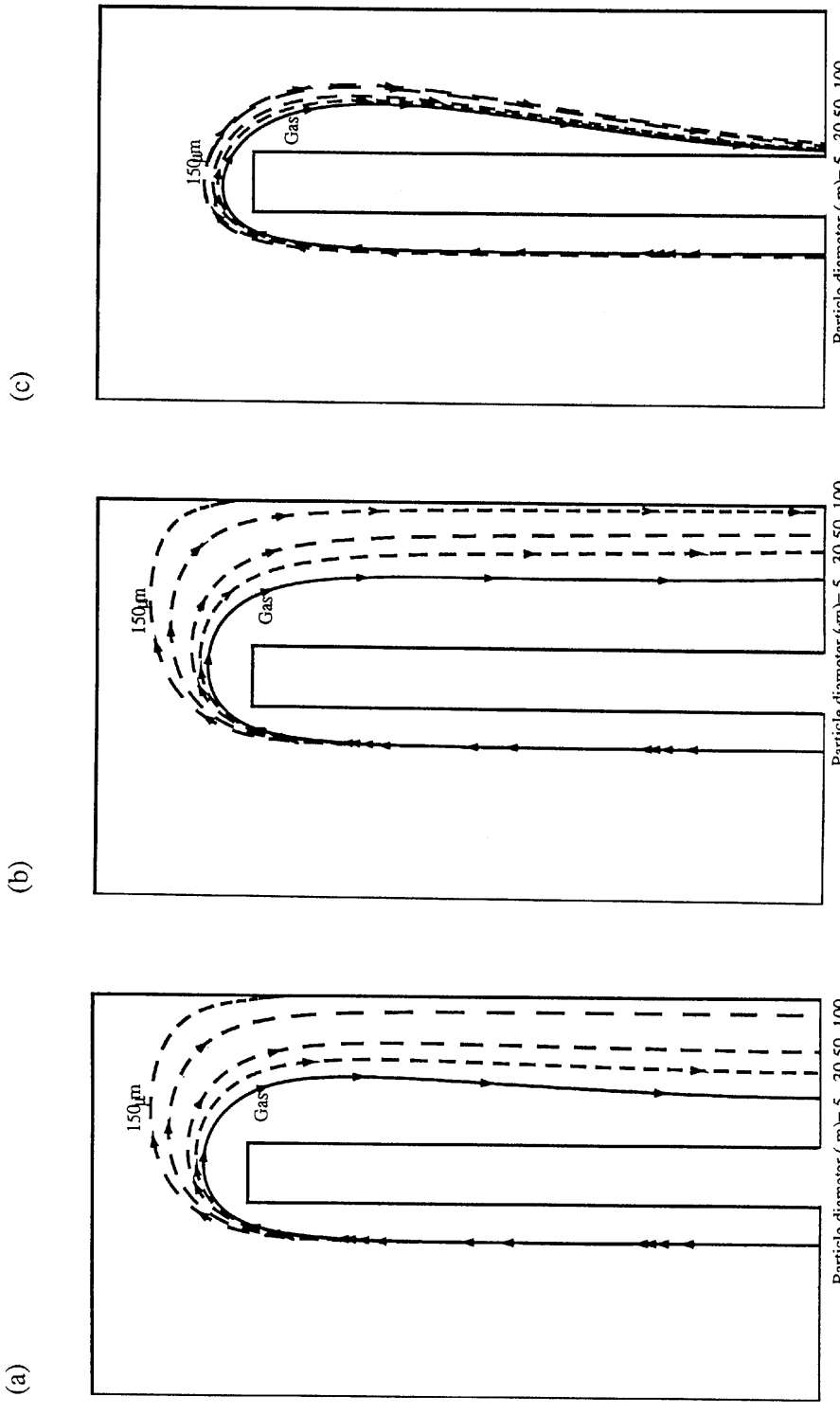

Figure 3. Particulate velocity streamlines (mean particle trajectories) for various particle sizes: (a) at symmetry plane (KPLANE = 2); (b) at mid-section between symmetry plane and rear wall (KPLANE = 16); (c) at plane near rear wall (KPLANE = 30)

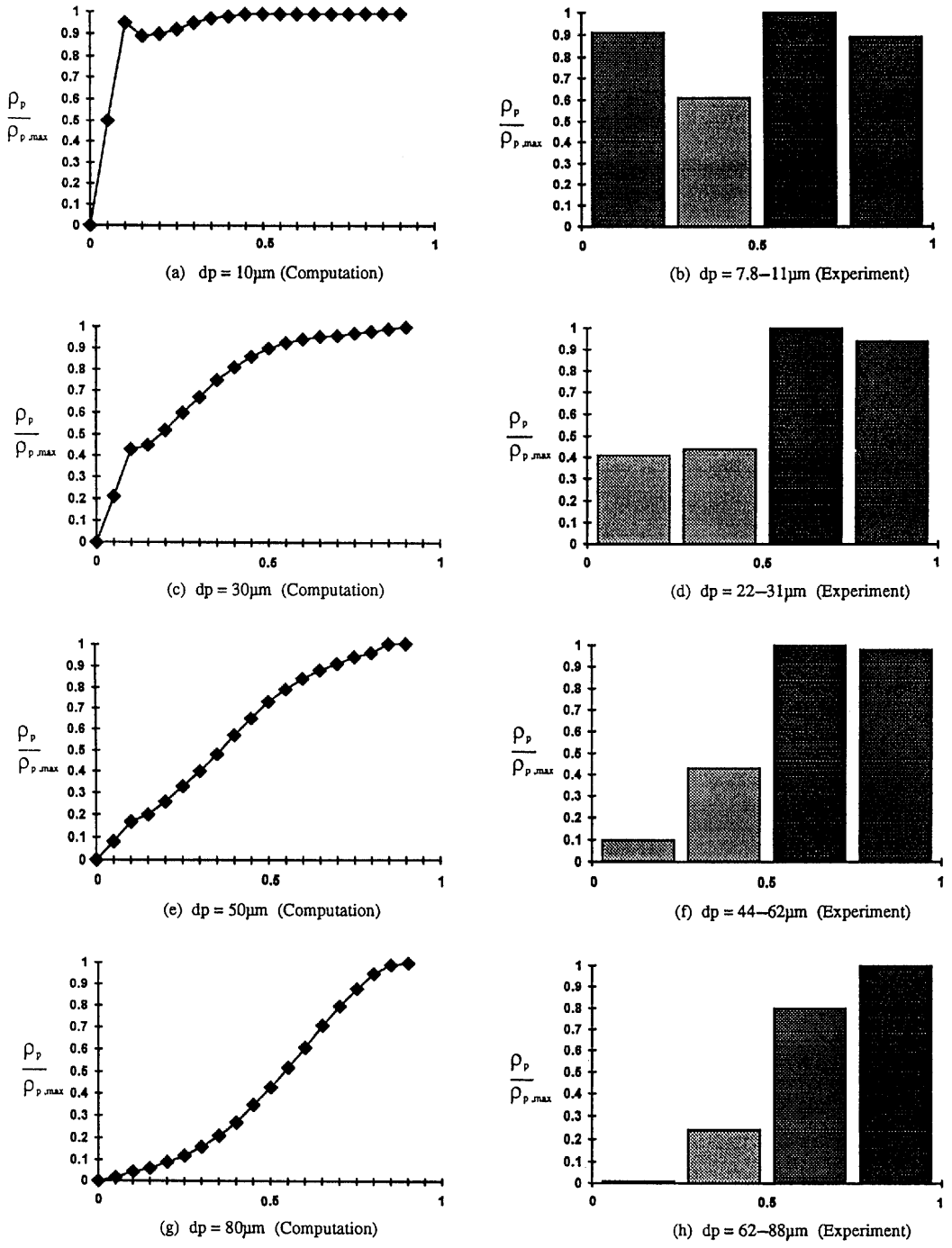

Figure 4. Comparison of particulate concentration at symmetry plane of economizer inlet with measured data;[22] 0, left wall; 1, right wall of inlet of economizer in lateral direction

Figure 4 gives a comparison of the particulate concentration distribution at the symmetry plane of the inlet of the economizer between the present computation and the measurements of Platfoot[22] in an operational power station. The co-ordinate in the vertical direction denotes the particulate concentration normalized by the maximum value for each group of particle sizes. In the lateral direction, 0 is at the left side of the economizer inlet and 1 corresponds to the right side. It is found from this figure that for the smaller particles (particle diameter less than $d_p = 10$ μm, corresponding to Stokes number $St = 0{\cdot}008$) the distribution of particles at the economizer inlet is quite uniform (some experimental error is expected in this group of measured data). With increasing particle size, the maximum values are shifted to the right-hand side. For the larger particles (particle diameter greater than $d_p = 80$ μm), very few particles can be found on the left side and most particles are flung to the right side of the economizer inlet adjacent to the outer wall. The computational results show very good agreement with the experimental measurements.

It is worthwhile noting that from our previous validation results[16,20,41,42] we find that using the RNG $k-\varepsilon$ model gives a better prediction than using the standard $k-\varepsilon$ model for most problems on a laboratory scale. However, it is hard to see any big difference when using the two different turbulence models for simulating such a large-scale problem as the present one.

One of the main interests of the present study is to predict the distributions of particulate velocity and concentration at the inlet of the economizer where severe erosion often occurs. It is generally accepted, based on a number of experiments,[43] that the empirical form of the relative rate of surface erosion could be

$$E \propto K\rho_p W_i^n f(\beta_i), \tag{35}$$

where K and n are constants depending on the physical characteristics of the materials involved ($n = 2-4$), ρ_p is the particle concentration, W_i is the incident particle velocity and β_i is the incidence angle. The numerical predictions of the information required in equation (35) at the inlet of the economizer are given in Figures 5–7 for various particle sizes ($d_p = 10$, 30 and 80 μm).

It should be noted that because the particle size $d_p = 10$ μm corresponds to a Stokes number $St = 0{\cdot}008$, Figure 5 also gives the flue gas behaviour at the inlet of the economizer. Looking at the velocity vector plots at the plane of the economizer entry (Figure 5(a)), we see that a recirculating area (secondary flow) is formed near the rear wall for smaller particles (also for the flue gas). It is observed that this recirculation zone is reduced with increasing particle size (see Figures 6(a) and 7(a). From the plots of velocity contours (Figures 5(b)–7(b) it can be seen that a peak velocity is found close to the rear wall. Comparing Figure 5(b) with Figure 7(b), we can see that larger particles are entering the economizer more slowly than smaller particles. As expected, the particulate concentration distribution is found to be quite uniform for smaller particles (see Figure 5(c)). With increasing particle size, more particles move into the economizer on the right side and more particles are found near the right wall and the rear wall (see Figures 6(c) and 7(c)). The incidence angle (defined between the entry plane and the velocity vector) of particles is also presented in Figures 5(d)–7(d). It could be concluded, according to the above fly-ash flow prediction and equation (35), that the maximum erosion for the top tubes of the economizer might occur in the area near the rear wall. The above information can be used for erosion prediction either using an accurate erosion model or as inlet boundary conditions to an erosion prediction computer programme.[44]

Figures 8 and 9 show the fly-ash velocity fields at three planes perpendicular to the economizer inlet for particle sizes $d_p = 30$ and 80 μm corresponding to $St = 0{\cdot}07$ and $0{\cdot}5$ respectively. It can be observed that a big recirculation zone is formed (see Figure 8(a)) at the plane near the inside of the

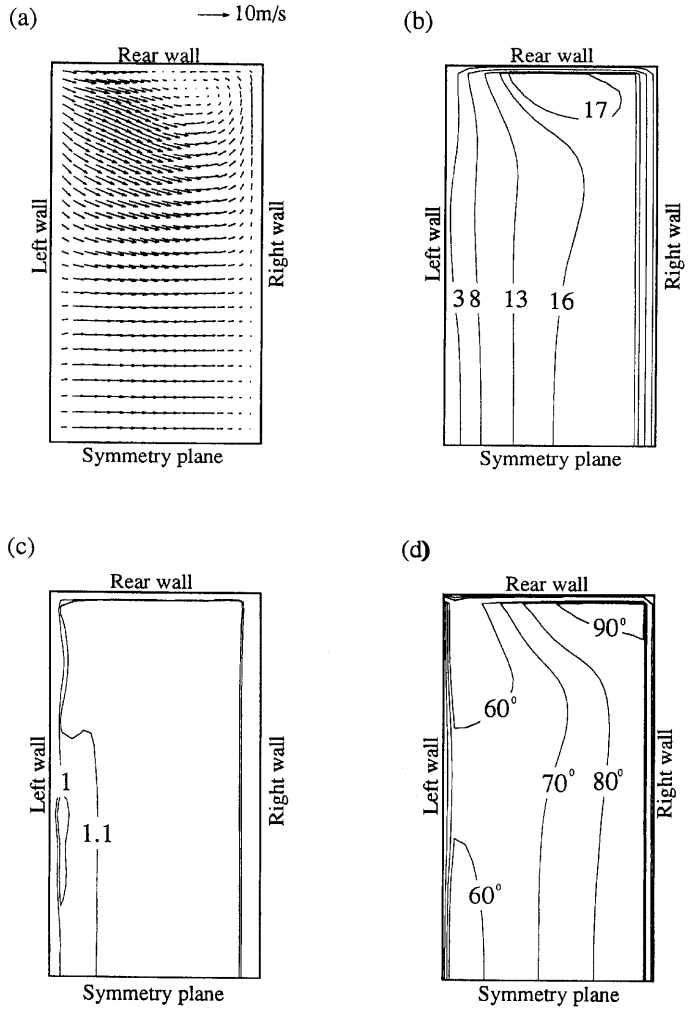

Figure 5. Computational results of particulate phase at plane of economizer inlet for $d_p = 10\ \mu$m: (a) velocity vectors (secondary flow); (b) vertical axial velocity contours (normal to plane of economizer inlet); (c) particle concentration contours (normalized by inlet particle concentration); (d) particle incidence angle (90° = normal to plane of economizer inlet)

bend. It is interesting to observe that for larger particles (see Figure 9(a)) two recirculation zones are found at the top of the boiler and in the economizer region respectively. The flow fields in the other sections are quite similar for the two different sizes of particles.

3.2. Boiler configuration II

A more realistic boiler configuration (boiler configuration II) is now considered. The three-dimensional computational domain and grids ($130 \times 32 \times 32$) for this case are illustrated in Figure 10. Figure 11 shows the numerical prediction of the flue gas through the boiler in terms of velocity

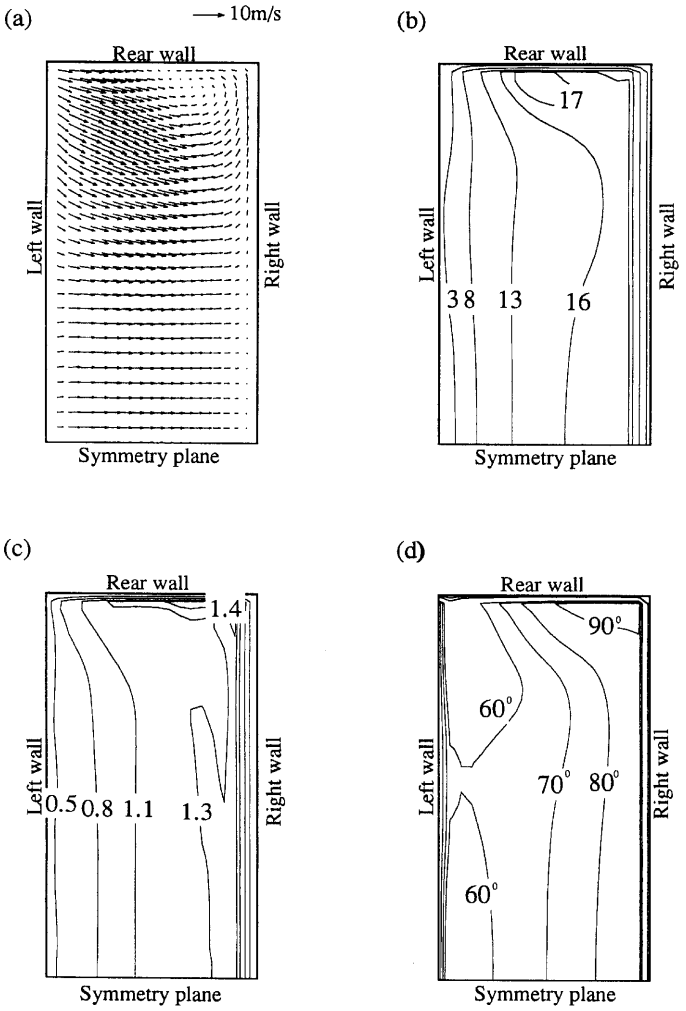

Figure 6. As Figure 5 but for $d_p = 30$ μm

vector plots at the symmetry plane and at a plane near the rear wall. At the symmetry plane we can see that the flue gas is accelerated at the top of the boiler and is centrifuged to the right side of the bend after turning through 180°. There is no recirculation zone observed at the inside of the bend. However, the flow pattern of the flue gas is significantly modified by the constraining effect of the rear wall. Owing to the three-dimensional effect, a secondary flow comes into the left corner of the top of the boiler. The flow is highly accelerated at the inside of the bend and a recirculation zone is formed there. Because very small fly-ash particles would entirely follow the flue gas flow, Figure 11 also gives the flow pattern of the lower-inertial fly-ash particles.

The fly-ash concentration contours (normalized) and velocity vector plots of the particulate phase are shown in Plate 1 for the symmetry plane and in Plate 2 for a plane near the rear wall. One may see that in Plate 1 (at the symmetry plane) both sizes of particles are centrifuged owing to the 180° bend

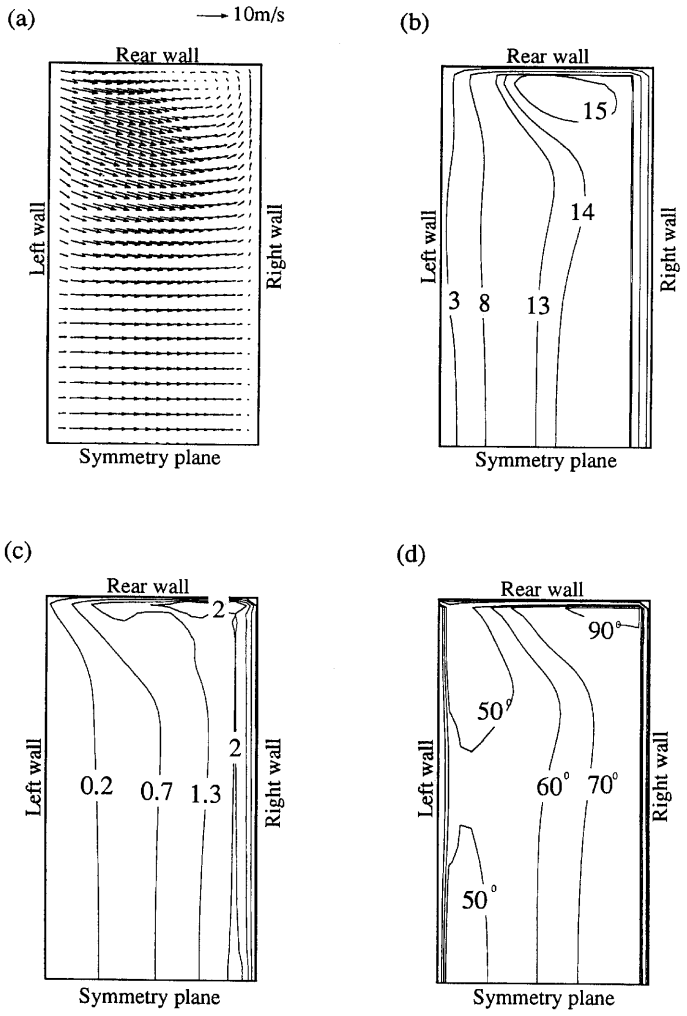

Figure 7. As Figure 5 but for $d_p = 80$ μm

and more fly-ash particles are flung to the outside of the bend, although, owing to the different inertia, a larger particle-free zone can be identified at the inside of the bend for high-inertia particles ($d_p = 80$ μm, $St = 0{\cdot}5$) than for lower-inertia particles ($d_p = 30$ μm, $St = 0{\cdot}07$).

It is interesting to notice, however, that in Plate 2 (at a plane near the rear wall) a high fly-ash concentration is observed for smaller particles ($d_p = 30$ μm, $St = 0{\cdot}07$) at the inside of the bend, which is contrary to the results at the symmetry plane. This is because the carrier flow (two-dimensional character at the symmetry plane) is further modified by the constraining effecting of the rear wall and the fluid flow strongly turns to generate a big recirculation zone at the inside of the bend. Since smaller fly-ash particles are more influenced by the fluid flow, more particles are turning along the inside of the bend and becoming entrained in the recirculation zone. However, it is still true that higher-inertial fly-ash particles ($d_m = 80$ μm, $St = 0{\cdot}05$) are less influenced by the fluid flow and most of them are thrown to the outside of the bend owing to the centrifugal effect. A large particle-free zone can still be identified at the inside of the bend.

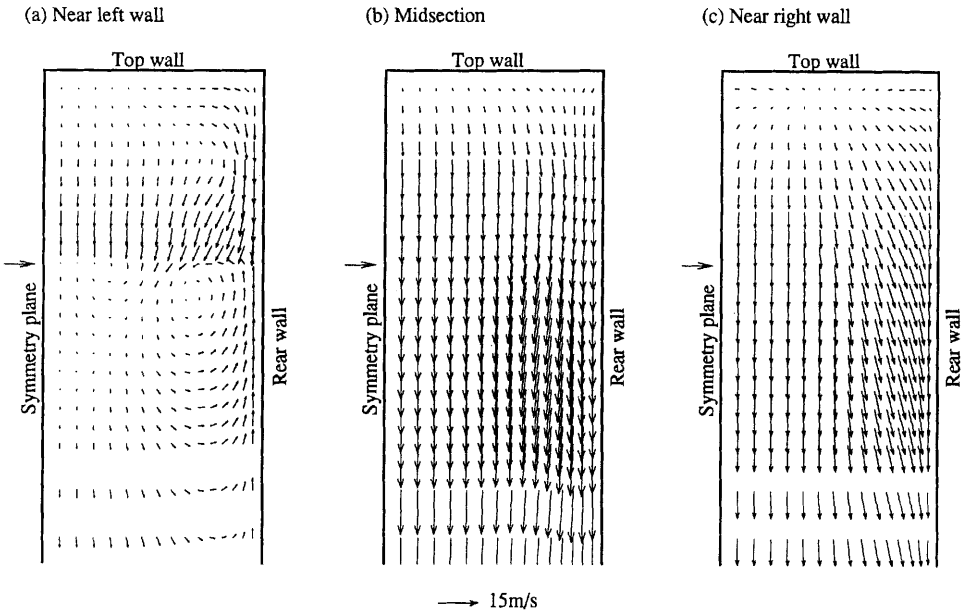

Figure 8. Fly-ash velocity fields for 30 μm particles at planes perpendicular to economizer inlet. Horizontal arrow indicates location of economizer inlet

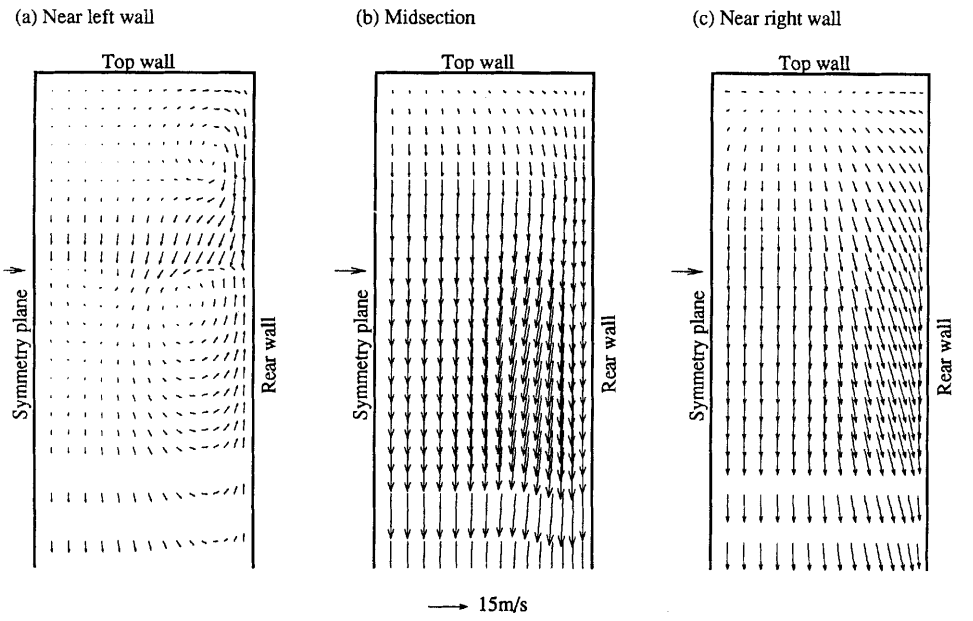

Figure 9. As Figure 8 but for 80 μm particles

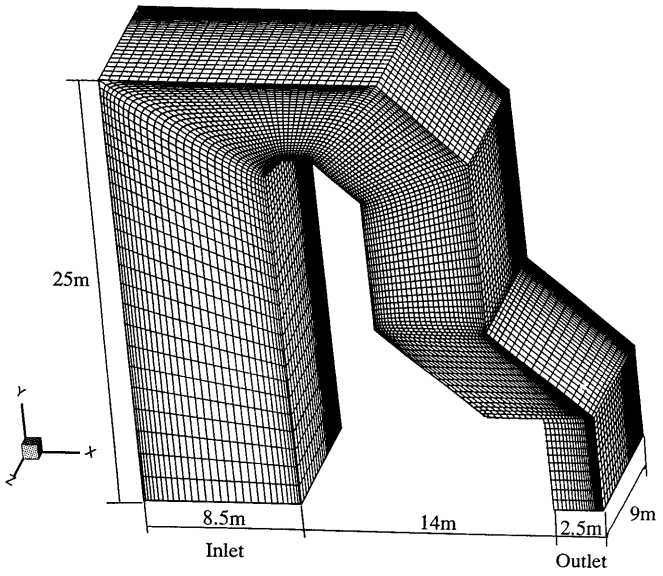

Figure 10. 3D schematic diagram of computational domain and grids for boiler model II

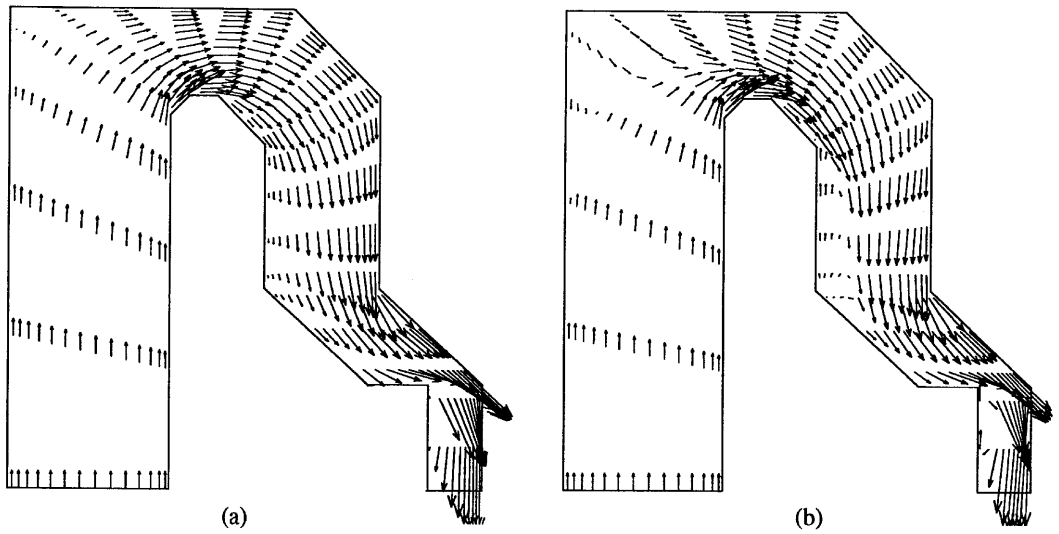

Figure 11. Velocity vector plots of flue gas: (a) at symmetry plane; (b) at plane near rear wall

4. CONCLUSIONS

A general three-dimensional approach based on a two-fluid model in combination with a developed particle–wall collision model and generalized Eulerian boundary conditions for the particulate phase is described for the treatment of turbulent gas–particle two-phase flows. An RNG-based $k-\varepsilon$ turbulence model with particulate turbulence modulation of the carrier gas phase is employed. The

method has been applied to the prediction of complex three-dimensional fly-ash flows in power utility boilers, which has not been reported in the literature previously. One of the main goals of the present study is to predict the mean flow field of the particulate phase (fly-ash) at the inlet of the economizer, where severe erosion often occurs. It is found that at the symmetry plane, very small fly-ash particles follow the gas flow and uniformly enter the economizer, while most of the larger fly-ash particles are flung to the right side of the economizer inlet. The numerical prediction of the fly-ash distribution at the economizer inlet is in very good agreement with the experimental measurements. However, this essentially two-dimensional character is further modified by the constraining effect of the rear wall. Most of the smaller fly-ash particles at a plane near the rear wall are flung to the left side of the economizer inlet, because the lower-inertial particles are more influenced by the flue gas flow which has been modified by the presence of the rear wall, while most of the larger fly-ash particles are still centrifuged and flung to the right side of the economizer inlet owing to their own higher inertia.

From the present prediction, a high concentration of fly-ash particles and maximum particulate velocity magnitude are observed in a region near the side wall of the boiler. According to an empirical erosion prediction formula, this suggests that severe erosion to boiler tubes might be found in this region of the boiler. The current information can be used for erosion prediction either using an accurate erosion model or as inlet boundary conditions to an erosion prediction computer programme. Subsequently, new designs of boiler configurations or erosion protection measures can be obtained through a parametric investigation.

ACKNOWLEDGEMENTS

The authors are grateful to DIST and Pacific Power (Electricity Commission of New South Wales, Australia) for the financial support provided as part of the DS4PUB project.

REFERENCES

1. W. P. Bauver, T. C. McGough and J. G. McGowan, 'A facility for the characterization of erosion of heat transfer tubing', in *Gas–Solids Flow*, ASEM, New Yor, 1984, pp. 115–122.
2. D. B. Murrary and J. A. Fitzpatrick, 'The effect of solid particles on crossflow heat transfer in a tube array', *Exp. Thermal Fluid Sci.*, **5**, 188–195 (1992).
3. ECNSW (Electricity Commission of New South Wales), 'Liddell power station unit 6: boiler rehabilitation', *Specification and Contract No. 3824*, 1988.
4. S. Elghobashi, 'On predicting particle-laden turbulent flows', *Appl. Sci. Res.*, **52**, 309–329 (1994).
5. C. P. Chen and P. E. Wood, 'A turbulence closure model for dilute gas–particle flows', *Can. J. Chem. Eng.*, **63**, 349–360 (1985).
6. A. Adeniji-Fashola and C. P. Chen, 'Modelling of confined turbulent fluid–particle flows using Eulerian and Lagrangian schemes', *Int. J. Heat Mass Transfer*, **33**, 691–701 (1990).
7. J. Y. Tu and C. A. J. Fletcher, 'An improved model for particulate turbulence modulation in confined two-phase flows', *Int. Commun. Heat Mass Transfer*, **21**, 775–783 (1994).
8. M. Y. Louge, E. Mastorakos and J. T. Jenkins, 'The role of particle collisions in pneumatic transport', *J. Fluid Mech.*, **231**, 345–359 (1991).
9. W. K. Melville and K. N. C. Bray, 'A model of the two-phase turbulent jet', *Int. J. Heat Mass Transfer*, **22**, 647–656 (1979).
10. M. Di, Giacinto, F. Sabetta and R. Piva, 'Two-way coupling effects in dilute gas–particle flow', *ASME J. Fluids Eng.*, **104**, 304–312 (1982).
11. R. Saurel, A Forestier, D. Veyret *et al.*, 'A finite volume scheme for two-phase compressible flows[, *Int. j. numer. methods fluids*, **18**, 803–819 (1994).
12. C. Masson and B. R. Baliga, 'A control-volume finite element method for dilute gas–solid particle flows', *Comput. fluids*, **23**, 1073–1096 (1994).
13. M. W. Reeks, 'On the constitutive relations for dispersed particles in nonuniform flows. 1: Dispersion in a simple shear flow', *Phys. Fluids A*, **5**, 750–763 (1993).

14. O. Simonin, E. Deutsch and M. Boivin, 'Large eddy simulation and second-moment closure model of particle fluctuating motion in two-phase turbulent shear flows', F. Durst *et al.* (eds), *Proc. Ninth Symp. on Turbulent Shear Flows*, Springer, New York, 199X.
15. J. Y. Tu and C. A. J. Fletcher, 'Eulerian Modelling of dilute particle-laden gas flows past tubes', *DS4PUB Tech. Rep. 94-11*, CANCES, University of New South Wales, Sydney, (1994).
16. J. Y. Tu and C. A. J. Fletcher, 'Numerical computation of turbulent gas–solid particle flow in a 90° bend', *AIChE J.*, **41**, 2187–2197 (1995).
17. M. O. Schweitzer and J. A. C. Humphrey, 'Note on the experimental measurement of particle flux to one and two in-line tubes', *Wear*, **126**, 211 (1988).
18. Y. Kliafas and M. Holt, 'LDV measurements of a turbulent air–solid two-phase flow in a 90° bend', *Exp. Fluids*, **5**, 73–85 (1987).
19. Y. S. Morsi, D. D. Atapattu and W. Yang, 'Experimental investigation of particle-laden gas flow through a tube bank', submitted.
20. J. Y. Tu, C. A. J. Fletcher, Y. S. Morsi *et al.*, 'Numerical and experimental studies of turbulent particle-laden gas flows in tube banks', submitted.
21. Y. Tsuji, Y. Morikawa and H. Shiomi, 'LDV measurements of an air–solid two-phase flow in a vertical pipe', *J. Fluid Mech.*, **139**, 417–434 (1984).
22. R. A. Platfoot, 'Internal flows in coal fired boilers', *Ph.D. Thesis*, Department of Mechanical Engineering, University of Sydney, 1991.
23. J. O. Hinze, 'Turbulent fluid and particle interaction', *Prog. Heat Mass Transfer*, **6**, 433–452 (1972).
24. J. Y. Tu and C. A. J. Fletcher, 'Continuum hypothesis in the computation of gas–solid flows', in D. Leutloff and R. C. Scrivastava (eds), *Computational Flud Dynamics*, Springer, Heidelberg, 1995, pp. 1–11.
25. D. A. Drew, 'Mathematical modelling of two-phase flow', *Ann Rev. Fluid Mech.*, **15**, 261–291 (1983).
26. M. J. Schuh, C. A. Schuler and J. A. C. Humphrey, 'Numerical calculation of particle-laden gas flows past tubes', *AIChE J.*, **35**, 466–480 (1989).
27. S. Ilias and P. L. Douglas, 'Inertial impaction of aerosol particles on cylinders at intermediate and high Reynolds numbers', *Chem, Eng. Sci.*, **44**, 81–99 (1989).
28. B. E. Launder and D. B. Spalding, 'The numerical computation of turbulent flows', *Comput. Methods Appl. Mech. Eng.*, **3**, 269–289 91974).
29. S. L. Soo, 'Development of theories on liquid solid flows', *J. Pipeline*, **4**, 137–145 (1984).
30. M. Sommerfeld, 'Modelling of particle–wall collisions in confined gas–particle flows', *Int. J. Multiphase Flow*, **18**, 905–926 (1992).
31. S. A. Orszag, V. Yakhot and W. s. Flannery, 'Renormalization group modelling and turbulence simulations', in R. M. C. So, C. G. Speziale and B. E. Launder (eds), *Near-Wall Turbulent Flows*, Elsevier, 1993, pp. 1031–1046.
32. L. Martinelli and V. Yakhot, 'RNG-based turbulence transport approximations with applications to transonic flows', *AIAA Paper 89-1950*, 1989.
33. G. Hetsroni, 'Particle–turbulence interaction', *Int. J. Multiphase Flow*, **15**, 735–746 (1989).
34. C. A. J. Fletcher, 'Gas particle industrial flow simulation using RANSTAD', in R. Narasimha (ed.), *Surveys in Fluid Mechanics*, Vol. 18, Parts 3 and 4, Indian Academy of Science, 1993, pp. 657–681.
35. N. -H. Cho and C. A. J. Fletcher, 'Computation of turbulent conical diffuser flows using a non-orthogonal grid system', *Comput. Fluids*, **19**, 347–361 (1991).
36. N. -H. Cho, C. A. J. Fletcher and k. Srinivas, 'Efficient computation of wing body flows', in *Lecture Notes in Physics*, Vol. 371, New York, 1991, pp. 167–191.
37. C. A. J. Fletcher and J. G. Bain, An approximate factorisation explicit method for CFD', *Comput. Fluids*, **19**, 61–74 (1991).
38. J. P. Van Doormaal and G. D. Raithby, 'Enhancements for the SIMPLE method for predicting incompressible fluid flow', *Numer. Heat Transfer*, **7**, 147–163 (1984).
39. C. M. Rhie and W. L. Chow, 'Numerical study of the turbulent flow past an airfoil with trailing edge separation', *AIAA J.*, **21**, 1525 (1983).
40. C. A. J. Fletcher, *Computational Techniques for Fluid Dynamics*, Vol. 2, *Specific Techniques for Different Flow Categories*, 2nd edn, Springer, Heidelberg, 1991.
41. J. Y. Tu and C. A. J. Fletcher, 'Computational analysis of turbulent gas–solid particle flows over tube banks', in *Gas–Solid Flow*, FED Vol. 228, ASME, New York, 1995, pp. 309–320.
42. J. Y. Tu and C. A. J. Fletcher, 'Computational modelling of particle dispersion in a backward-facing step flow', *Proc. 2nd Int. Symp. on Numerical Methods for Multiphase Flows/1996 ASME-FED Summer Meet.*, San Diego, CA, ASME, New York, 1996.
43. J. A. C. Humphrey, 'Review—fundamentals of fluid motion in erosion by solid particle impact', *Int. J. Heat Fluid Flow*, **11**, 170–195 (1990).
44. F. C. Christo and C. A. J. Fletcher, 'Erosion modelling in Vales Point power station using ''ECONEROS'' code', *Tech. Rep. to Pacific Power Corporation*, Department of Mechanical Engineering, University of Sydney, 1992.

